Advances in Water Resources 64 (2014) 47–61

Contents lists available at ScienceDirect

Advances in Water Resources

journal homepage: www.elsevier.com/locate/advwatres

Binary upscaling on complex heterogeneities: The role of geometry and connectivity

F. Oriani *, P. Renard

Centre of Hydrogeology and Geothermics, University of Neuchâtel, 11 Rue Emile Argand, CH-2000 Neuchâtel, Switzerland

ARTICLE INFO

Article history:
Received 11 April 2013
Received in revised form 20 December 2013
Accepted 22 December 2013
Available online 30 December 2013

Keywords:
Upscaling
Equivalent conductivity
Shape
Euler number
Connectivity
Percolation

ABSTRACT

The equivalent conductivity (K_{eq}) of a binary medium is known to vary with the proportion of the two phases, but it also depends on the geometry and topology of the inclusions. In this paper, we analyze the role of connectivity and shape of the connected components through a correlation study between K_{eq} and two topological and geometrical indicators: the Euler number and the Solidity indicator. We show that a local measure such as the Euler number is weakly correlated to K_{eq} and therefore it is not suitable to quantify the influence of connectivity on the global flux; on the contrary the Solidity indicator, related to the convex hull of the connected components, presents a direct correlation with K_{eq}. This result suggests that, in order to estimate K_{eq} properly, one may consider the convex hull of each connected component as the area of influence of its spatial distribution on flow and make a correction of the proportion of the hydrofacies according to that. As a direct application of these principles, we propose a new method for the estimation of K_{eq} using simple image analysis operations. In particular, we introduce a direct measure of the connected fraction and a non-parametric correction of the hydrofacies proportion to compensate for the influence of the connected components shape on flow. This model, tested on a large ensemble of isotropic media, provides a good K_{eq} approximation even on complex heterogeneities without the need for calibration.

1. Introduction

The adoption of Darcy's law for the description of a macroscopic flow through porous media is commonly accepted, but the problem of finding a representative hydraulic conductivity arises in the case of a heterogeneous medium. This type of problem and the proposed solutions are concerning all the physical processes which follow the same type of laws, e.g. electricity or heat conductance. Regarding hydrogeology, the subject is of primary importance for hydrocarbon reservoir and hydrological basins flow modeling, since local parameterization needs to be conveniently upscaled to represent large-scale properties in the model. The upscaling can be done by substituting each volume of heterogeneous sediments with a homogeneous medium characterized by an equivalent hydraulic conductivity (K_{eq}) value in order to present the same mean flow response. In a complex aquifer, this value is a function of the small-scale hydraulic conductivities and the proportion of each hydrofacies, but also of their sub-scale geometry [1]. The arithmetic and the harmonic mean of the local conductivities are known to be the widest upper and lower K_{eq} bounds respectively [2]. These bounds are referred to as Wiener bounds and correspond to the cases in which the flow is parallel or perpendicular to a set of plain layers of different conductivities. In the case of a binary and statistically isotropic medium, the K_{eq} range can be reduced to the Hashin–Shtrikman bounds [3]. The Effective Medium Theory (*EMT*), based on Maxwell formula [4] on spherical inclusions, gives an exact analytical solution for the effective conductivity K_{eff} of a very dilute suspension of inclusions in a homogeneous matrix of conductivity K_0, in which the mean flow is uniform and governed by the matrix. This formula, then developed by Matheron [5], Dagan [6,7] and applied to bimodal formations by Rubin [8], has been recently generalized for three-dimensional heterogeneous medium of log-normal distribution [9], giving an accurate approximation for denser configurations of the inclusions [10], different radius [11], shape and distribution [12]. The main limit of this approach lies in some assumptions that are not satisfied when the integral scale of the inclusions material is large with respect to the size of the upscaled volume, the non-linear interactions between the inclusions become more and more important and the estimation less accurate.

Many other approaches have been developed for the study and estimation of K_{eq} including for example, the stochastic theory applied to random multi-Gaussian fields [13,14], power averaging equations [15], homogenization theory [16] and renormalization [17,18]. For an extensive overview about these methods see [19,20]. These techniques give accurate results for specific types

* Corresponding author. Tel.: +41 32 718 25 63.
E-mail addresses: fabio.oriani@unine.ch (F. Oriani), philippe.renard@unine.ch (P. Renard).

0309-1708/$ - see front matter © 2013 Elsevier Ltd. All rights reserved.
http://dx.doi.org/10.1016/j.advwatres.2013.12.003

of heterogeneities and do not provide a thorough topological and geometrical analysis. Recently, the topology and geometry of the sub-scale structure has been recognized to be of crucial importance for the upscaled conductivity [21–25]. Knudby et al. [26] developed a model for the estimation of K_{eq} in random binary fields containing multiple inclusions. Their formula, derived from the empirical observations of Bumgardner [27], is based on a static connectivity measure: the mean distance between the inclusions along the mean flow direction. This approach leads to good estimations for fields presenting isolated inclusions however it is not flexible enough to deal with more complex heterogeneities, for instance channeled textures or non-convex inclusions penetrating each other. Finally, Herrmann and Bernabé [28,29] proposed a site percolation model for binary fields that accounts for the connectivity of the more conductive hydrofacies as a function of its proportion. This parametric approach can be applied on known stochastic fields, otherwise it has to be calibrated through physical or numerical experiments.

The aim of this paper is to analyze how the geometry and connectivity of heterogeneities influence the equivalent hydraulic conductivity (K_{eq}) of isotropic binary media. For this purpose, we perform an analysis of the correlation between K_{eq} and two topological and geometrical indicators: the Euler number and the Solidity indicator. This is done on a group of 2D binary fields which present a large variability of these indicators. Furthermore, we propose a new method based on image analysis to estimate K_{eq} for isotropic binary fields. The proposed algorithm is tested mainly on 2D fields, but an early 3D implementation of the algorithm is also presented. The proposed approach is essentially empirical. It finds its roots in the correlation studies and the analysis of the flow fields from numerical simulations. This method allows to rapidly estimate the equivalent, or "block", conductivity on any given isotropic binary field, using no information about the underling statistical model. The analysis is conducted on 2D realizations of stochastic fields and 3D natural heterogeneities without assuming stationarity, mean uniform flow or restrictions on the integral scale of the conductivity field.

The paper is organized as follows: in Section 2 the techniques used for the generation of the binary conductivity fields, the computation of the spatial indicators and the reference K_{eq} values are described. In Section 3, the results obtained from the correlation studies are presented and discussed. In Section 4, the new formula for the estimation of K_{eq} is presented together with its application on complex heterogeneities. Section 5 is devoted to conclusions.

2. Materials and methods

In this section, we describe the different steps required to make a quantitative analysis of the influence of geometry and topology on the equivalent conductivity and develop a K_{eq} estimation model. The preliminary part consists in the generation of several groups of two-dimensional binary fields, presenting isotropic textures and varying proportion, shape and connectivity values for each hydrofacies. This gives us a wide basis for our correlation study. Second, the equivalent conductivity is computed performing flow simulations on the generated fields and it is used as reference. Third, the Euler number of the more conductive hydrofacies is calculated for each field and adopted as connectivity indicator. Fourth, the average Solidity indicator is computed and used as a geometrical indicator. Finally, a correlation study between K_{eq} and these indicators is performed and an experimental algorithm to estimate K_{eq} based on image analysis is proposed as an application of the information achieved through the correlation study.

2.1. Generation of binary fields

The binary fields used in this study are composed of a highly permeable material (represented by the symbol *HP* in the rest of the text, the value 1 in the binary fields and the white color in the figures) with a hydraulic conductivity value $k_h = 5 \times 10^{-2}$ (m/s) and a less permeable one (*LP*, value 0, black color) with $k_l = 5 \times 10^{-6}$ (m/s). In the first part of the study the aim is to vary one spatial indicator at a time (e.g. varying the Euler number and keeping constant the Solidity indicator and the hydrofacies proportion) in order to investigate its correlation with K_{eq}. This is achieved by adding randomly placed non-touching inclusions of one hydrofacies on a clean background until the desired proportion p of the inclusions is reached. In this way, one can control the level of connectedness indirectly by varying the dimension, number and minimal distance between the connected components, while keeping a constant proportion p, or control the geometry choosing among any type of shape (Table 1, tests 1 and 2). In the second part, the aim is to test the new method of K_{eq} estimation as systematically as possible on fields presenting both simple and complex geometries. For this purpose, a group of 2D Bernoulli fields (Table 1, test 3) is obtained by imposing different threshold values on 400 arrays composed of uniformly distributed pseudo-random numbers. All the range of proportion $p \in [0, 1]$ is covered and the obtained fields are statistically isotropic.

Moreover, we generate 10,800 binary images presenting various types of texture with the following procedure (Table 1, test 4):

1. We start from a group of 20 realizations of a 2D multivariate Gaussian random model, simulated using a Gaussian variogram with a correlation length of 40 pixels.
2. Using the technique proposed by Zinn and Harvey [22], each realization is transformed to obtain two different fields: in the first one, continuous channels are formed by the minima of the 2D multivariate Gaussian random function and, in the second one, the same type of structures are formed by the maxima.
3. 18 combinations of coupled threshold values are imposed on each field to obtain different types of binary, generally well connected, distributions. In order to maximize the geometrical and topological variability among the binary images, the threshold values are computed as $T = (D + S)/2$, where D is a vector of values taken at regular intervals in the range of the generated variable and S is a vector of equally distant quantiles of its empirical probability distribution.
4. Finally, each of these images is edited using the matlab function *Randblock* (Copyright 2009 Jos vander Geest), which divides the image in squares of the same size and randomly mixes them. We use this tool to obtain several fields with the same material proportions but different geometries and connectivities. This operation is repeated 10 times, progressively reducing the square size to obtain finer textured mosaics.

This ensemble of techniques allows to cover the space of the possible (p, K_{eq}) solutions widely (see Section 4.1). Even if the starting images are isotropic, using Randblock may cause the formation of anisotropic media. For this reason, the fields presenting a ratio between the principal components of the reference K_{eq} tensor (see Section 2.2) out of the interval (0.5–2) are excluded from the study. This operation reduces the number of fields to 10,216.

Finally, the resolution of each image is augmented from 100×100 to 400×400 pixels in order to reduce the numerical error in the flow simulations that may be caused by connected components presenting a width inferior to 3 pixels.

The last test (Table 1, test 5) is done on 2196 3D binary fields of size $100 \times 100 \times 100$, obtained from an ensemble of micro-computerized-tomography (micro-CT) images of micro-metric sandstone, carbonate, synthetic silica and sand samples (Imperial College of London [30]). The aim of this test is not to give a credible $\mathbf{K}_{eq}$ estimation related to these materials, which should be done using pore-scale modeling techniques, but to have some initial

Table 1
Summary of the generated fields, with the imposed values of proportion (p), Euler number (E) and Solidity indicator (S). The values may be fixed ($\{\cdot\}$) or vary in a certain interval ($(\cdot)$,$[\cdot)$, etc.). The intervals of possible values for a finite raster image are shown in the header.

Test	Description	Number of images	p [0,1]	E $(-\infty,+\infty)$	S (0,1]
1	Rectangular *LP* and *HP* inclusions	960	{0.81, 0.18}	$(-\infty,+\infty)$	{1}
2	*LP* and *HP* inclusions, various shapes	1680	{0.64, 0.36}	{−40,41}	(0,1]
3	Bernoulli fields	400	[0,1)	a	a
4	Complex geometries	10216	(0,1)	a	a
5	3D micro-CT images	2196	(0,1)	a	a

a = The parameter is not controlled.

feedback of the application of the principles exposed in this paper on three-dimensional isotropic fields. This group includes several natural binary textures, showing different levels of connectivity of the two materials. To exhaustively cover the possible range of proportion, the phase-inversion of the fields has also been considered, but only the isotropic ones have been selected, according the same criterion used for test 4.

2.2. Estimation of the equivalent conductivity using flow simulations

Following Rubin and Gómez-Hernández [31], we compute the equivalent conductivity tensor of each binary field by solving numerically the following equation:

$$\begin{aligned}&\frac{1}{V}\int_V \mathbf{u}\,\mathrm{d}v = -\mathbf{K}_{eq}\frac{1}{V}\int_V \nabla h\,\mathrm{d}v\\ &\langle\mathbf{u}\rangle = -\mathbf{K}_{eq}\langle\mathbf{j}\rangle,\quad \mathbf{j}=\nabla h\end{aligned} \tag{1}$$

where V is the total volume of the medium, $\mathbf{u}$ the specific flux vector and $\mathbf{K}_{eq}$ the equivalent conductivity tensor. For 2D fields, two numerical flow simulations are performed on a regular squared grid using the finite element method (*FEM*) implemented in the *Ground Water* library [32]. It has to be remarked that *FEM* applied to this type of grid gives a discrete solution in $\prod_{i=1}^{N}(d_i+1)$ points for a N-dimensional local conductivity matrix of size $\mathbf{d}$. This solution represents also the diagonal flow paths between the elements, in accordance to the criterion adopted for the connectivity measures used this paper (see Section 2.3).

Permeameter-type boundary conditions are applied: the first simulation has a prescribed head $h = x$ along the vertical boundaries and no-flow conditions along the horizontal ones. This leads to a horizontal main flow direction with the following mean gradient and mean velocity vectors:

$$\langle\mathbf{j}\rangle = \begin{bmatrix}1\\0\end{bmatrix}\ \langle\mathbf{u}\rangle = \begin{bmatrix}K_{xx}\\K_{yx}\end{bmatrix} \tag{2}$$

Performing a second flow simulation with the same type of boundary conditions but turned perpendicularly, we obtain the complete equivalent conductivity tensor from (1):

$$\mathbf{K}_{eq} = \begin{bmatrix}K_{xx}K_{xy}\\K_{yx}K_{yy}\end{bmatrix} \tag{3}$$

The tensor is computed similarly in 3D fields obtaining a 3×3 matrix. $\mathbf{K}_{eq}$ is symmetric and diagonal for isotropic fields, which is the case for the ones used in this paper (with a reasonable approximation, see Section 2.1). The principal components of the obtained $\mathbf{K}_{eq}$ tensor are therefore considered the reference $\mathbf{K}_{eq}$ values.

2.3. Connectivity and the Euler number

In a digital image, which is a squared tessellation of a continuous space, connectivity can be related to the concept of path-connectedness through the definition of neighborhood. A 2D digital image is an array Π of lattice points having positive integer coordinates $\mathbf{x}=(x,y)$, where $1\leqslant x\leqslant M$ and $1\leqslant y\leqslant N$. Following [33], for each point (x,y), we consider two types of neighborhoods: the *4-neighbors*, which are the four horizontal and vertical adjacent points $(x,y\pm1)$ $(x\pm1,y)$, and the *8-neighbors*, which are the
4-neighbors plus the points $(x+1,y\pm1)$ and $(x-1,y\pm1)$. A path between two points p and q of Π can be defined as a sequence of points $(p_i)=(p_0,p_1,\ldots,p_n)$ such that $p_0=p, p_n=q$ and p_i is a neighbor of p_{i-1}, $1\leqslant i\leqslant n$. G being a non-empty subset of Π, two points p and q of G are said to be *connected in G* ($p\overset{G}{\leftrightarrow}q$) if a path (p_i) with $i=0,1,\ldots,n$ exits from p to q such that $(p_i)\subseteq G$. According to the type of neighborhood adopted in defining the path, we can talk about *4* or *8-connected* points.

For a matter of consistency in connectivity (the Jordan curve theorem [34]), we cannot consider the same type of neighborhood for both G and its complement in Π ($\bar{G}$). Therefore, for a two-dimensional square lattice, the possible connectivities are the $[8,4]$, i.e. considering the 8-neighbors for G and the 4-neighbors for $\bar{G}$ and the opposite one $[4,8]$. In this paper, where the G and $\bar{G}$ represent *HP* and *LP* respectively, the $[8,4]$ connectivity is adopted, since punctual contacts of *HP* result to be locations of high-velocity flow paths, as seen from the output velocity fields of the flow simulations. For the 3D case, the $[26,6]$ connectivity is adopted, i.e. considering all the voxels in the 3×3 neighborhood cell for the *HP* material and only the ones sharing an entire face for the *LP* material.

Moreover, the largest disjoint non-empty subsets of G satisfying the equivalence relation $p\overset{G}{\leftrightarrow}q$ are called *connected components of G*. Roughly speaking, a connected component is an isolated portion of a given material. A connected component of $\bar{G}$ which does not contain the borders of Π, i.e. totally surrounded by G, is called a *hole in G*.

The Euler number is a topological indicator which quantifies the connectivity of a space (representing a medium here) in n dimensions. On the basis of the previous definitions, for a two-dimensional subset G of Π, it can be defined by the following relation [35]:

$$E = n_0 - n_1, \tag{4}$$

where n_0 is the number of connected components of G and n_1 the total number of holes in G. Well connected spaces have negative E values, whereas poorly connected spaces have positive values. For example, if we add a path between two connected component obtaining a single one, we reduce n_0, or, if we add two distinct paths, we obtain a single connected component with a hole inside, reducing n_0 and augmenting n_1. Doing this kind of operations leads to lower E values and an increased connectivity.

In this paper, the computation of E is performed using the matlab function *bweuler* (Copyright 1993–2005 The MathWorks, Inc., based on [36]). For topological and geometrical measures in two-dimensional digital images see [33,37].

2.4. Computation of the Solidity indicator

In a binary field, the flow is influenced by the two hydrofacies distributions. This level of interaction is not only a function of the proportion and connectivity but also of the shape of the connected components. This is obvious when looking at Fig. 1, which represents four binary distributions with a *HP* matrix and *LP* inclusions. Fields 1 and 3 have similar p and E values and so have fields 2 and 4. Their respective specific flux fields are shown below, the boundary conditions are described in Section 2.2 such that the average hydraulic gradient magnitude is $\langle | \mathbf{j} | \rangle = 1$, with the main flow directed from top to bottom. In these conditions, the portions which are far from the hydrofacies transition present a local specific flux magnitude $| \mathbf{u} | \sim k_h$ (gray areas) for the *HP* material and $| \mathbf{u} | \sim k_l$ (black areas) for *LP* material, i.e. they correspond to undisturbed zones where the flow response is the same as a homogeneous medium. On the other hand, the *HP* material near the *LP* inclusions is subjected to a local gradient $| \mathbf{j} | \neq 1$ and a subsequent increase or decrease of *k*, creating higher (red) or lower (blue) velocity zones. In particular, if the inclusions are convex, the red and blue zones are equally present in the medium, compensating their influence to the mean flow (fields 1 and 2). On the contrary, if the shape of the inclusions is very articulated (fields 3 and 4), the blue zones cover a wider region than the red ones and the mean flow through the medium is low.

The opposite phenomenon is present in fields composed of a *LP* matrix with *HP* inclusions: when their shape is more articulated, they allow the flow to force its way up the *LP* matrix, creating higher velocity paths.

To quantify this effect, we propose to use the *Solidity* indicator *S*. It is defined for a given connected component *CC* as the ratio between its area (*A*) and its convex hull (*H*), which corresponds to the smallest convex polygon containing *CC*. *S* varies from values close to 0 for very articulated shapes, to 1 for convex shapes. In our correlation study, we consider the average value over all the inclusions:

$$S = \frac{1}{N} \sum_{i=1}^{N} A_i / H_i \tag{5}$$

where A_i is the area of the *i*th inclusion, H_i its convex hull and *N* the total number of inclusions. This is computed for *LP* inclusions in a *HP* matrix and vice versa. The indicator *S* is calculated using the matlab function *regionprops* (Copyright 1993–2008 The MathWorks, Inc., based on [38]).

3. The impact of connectivity and shape on K_{eq}

In this section the influence of connectivity and shape of the connected components on the equivalent conductivity is investigated through the correlation study with the Euler number and the Solidity indicator.

3.1. Correlation between the Euler number and the equivalent conductivity

Fig. 2 shows the results of test 1. In this numerical experiment, the equivalent conductivity is only weakly correlated with the Euler number. Inside each of the two groups of fields (Fig. 2 top and bottom respectively), K_{eq} presents only small variations due to the position of the connected components with respect to each others or to the boundaries of the fields. This observation is supported by the fact that this variability is strongly reduced going toward higher absolute *E* values, where the number of inclusions increases and the mean distance among each other becomes constant, as well as in the case of $E = 0$ or $E = 1$, where there is only one inclusion. More importantly, this experiment is clear evidence of the inefficiency of any local connectivity measure in predicting a variation of the mean global flow: any indicator based on the neighborhood of each pixel or on the number of connected components, as the Euler number does, would show here a dramatic distance between the fields, which does not correspond to a significant K_{eq} variation. On the contrary, there exists a considerable variation in the mean global flow between the two groups, related to the presence in the second group of the percolating *HP* cluster, i.e. the portion of *HP* connecting the opposite borders of the fields. Its presence determines a K_{eq} increase of four orders of magnitude. In conclusion, a connectivity measure relying on the quantification of the percolating *HP* cluster (see the model proposed in Section 4) may lead to a better prediction of the mean global flow through the medium. It has to be noted that such a measure is still based on the topological definition of path-connectedness, but it is applied globally, since it requires isolation of the *HP* connected components which form connected paths between the boundaries of the entire medium. Moreover, it involves a quantification of the number of pixels belonging to this region, an operation which goes beyond the topological characterization of the domain.

3.2. Correlation between the Solidity indicator and the equivalent conductivity

The results of test 2 (Fig. 3) are the following: when the proportion of the two hydrofacies is kept constant, the shape of the inclusions has a significant influence on K_{eq} and shows a clear

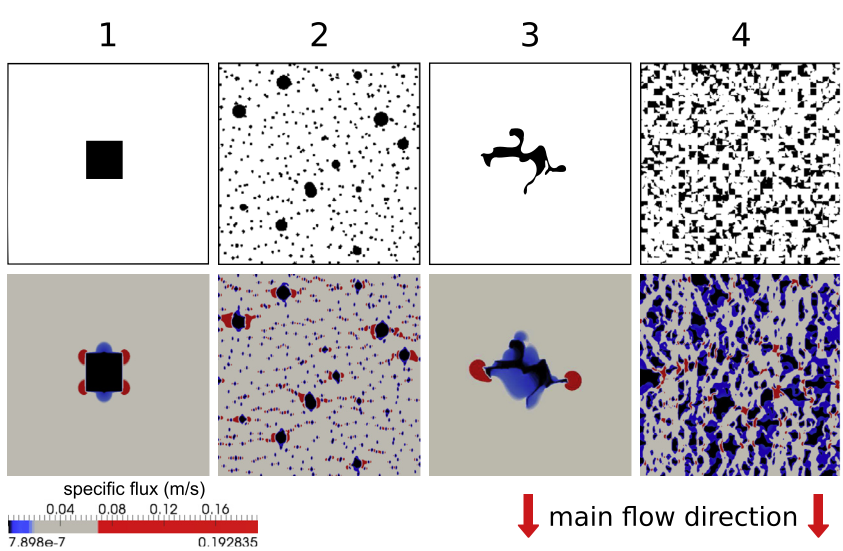

Fig. 1. Example of binary distributions with non conductive inclusions: with convex (1) and (2) and articulated (3) and (4) shapes. Below: the respective specific flux magnitude field with the main flow directed from top to bottom.

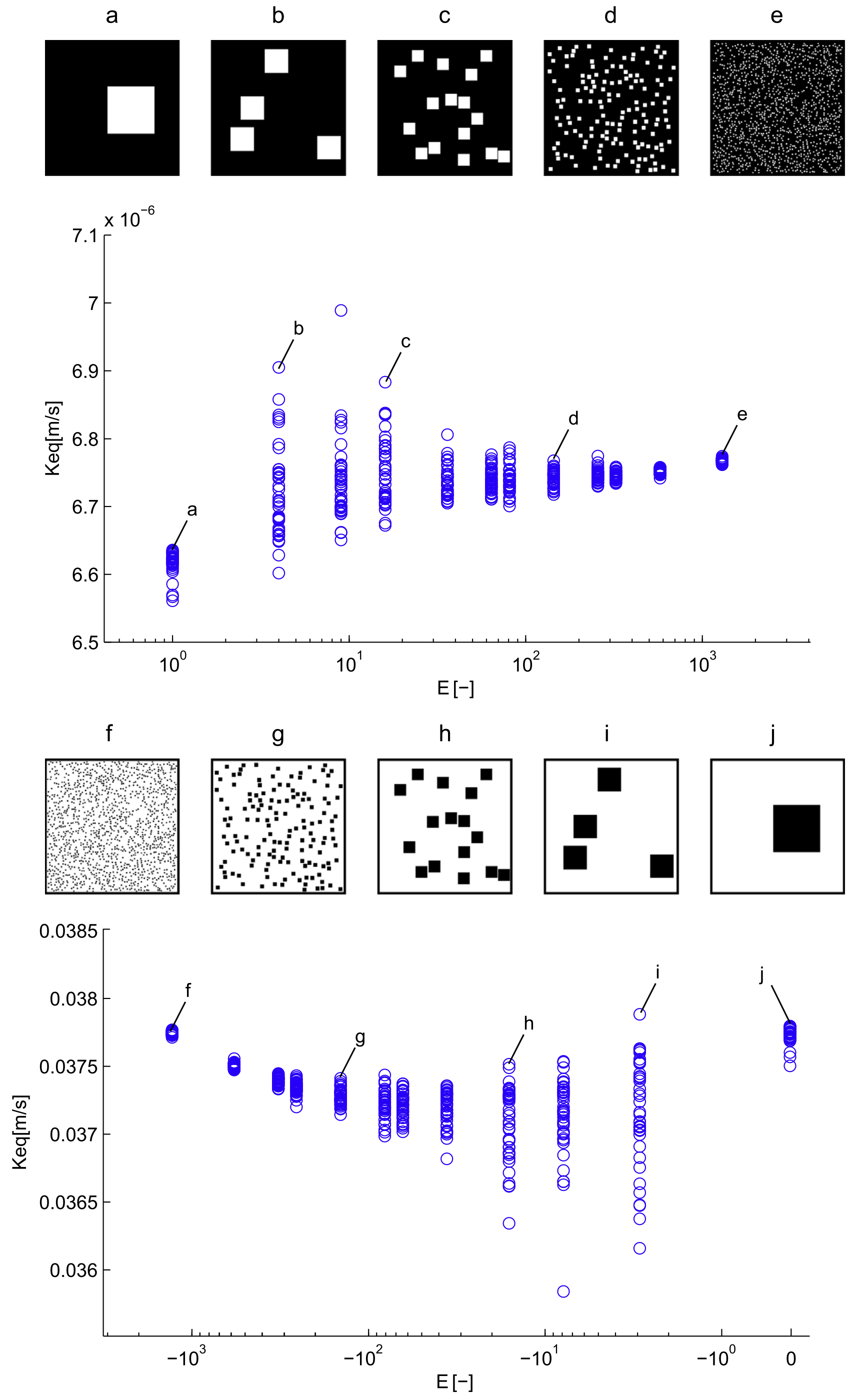

Fig. 2. Test 1, correlation between E (computed on *HP*) and K_{eq} (geometric mean of x and y components): *HP* inclusions in a *LP* matrix (top), *HP* matrix presenting *LP* inclusions (bottom). A hybrid log/linear scale is adopted in order to show $E = 0$.

non-linear correlation with it. In particular, fields presenting *LP* inclusions show a positive correlation between K_{eq} and S, while a negative correlation is observed in fields with *HP* inclusions. The small variability inside each group of fields presenting the same S can be explained, similarly to test 1 (Section 3), with the influence of the relative position of the connected components, still present but less significant compared to the role of the shape.

A strong advantage of the Solidity indicator is that it is dimensionless and invariant to the dimensions of the connected components, thus easy to introduce as a parametric shape correction. Moreover, it is less prone to local noise, since the convex hull of a connected component does not change significantly depending on its small-scale features as little holes or rugged surfaces. On the other hand, being a local measure, it should be weighted accounting for each connected component area with respect to the field size to obtain a more precise parametric measure. In case of finer textures, this operation may significantly raise the computation time. In general, the important finding given by this correlation study is that the area of influence of each inclusion can be represented by its convex hull and different geometries may significantly influence the K_{eq} value.

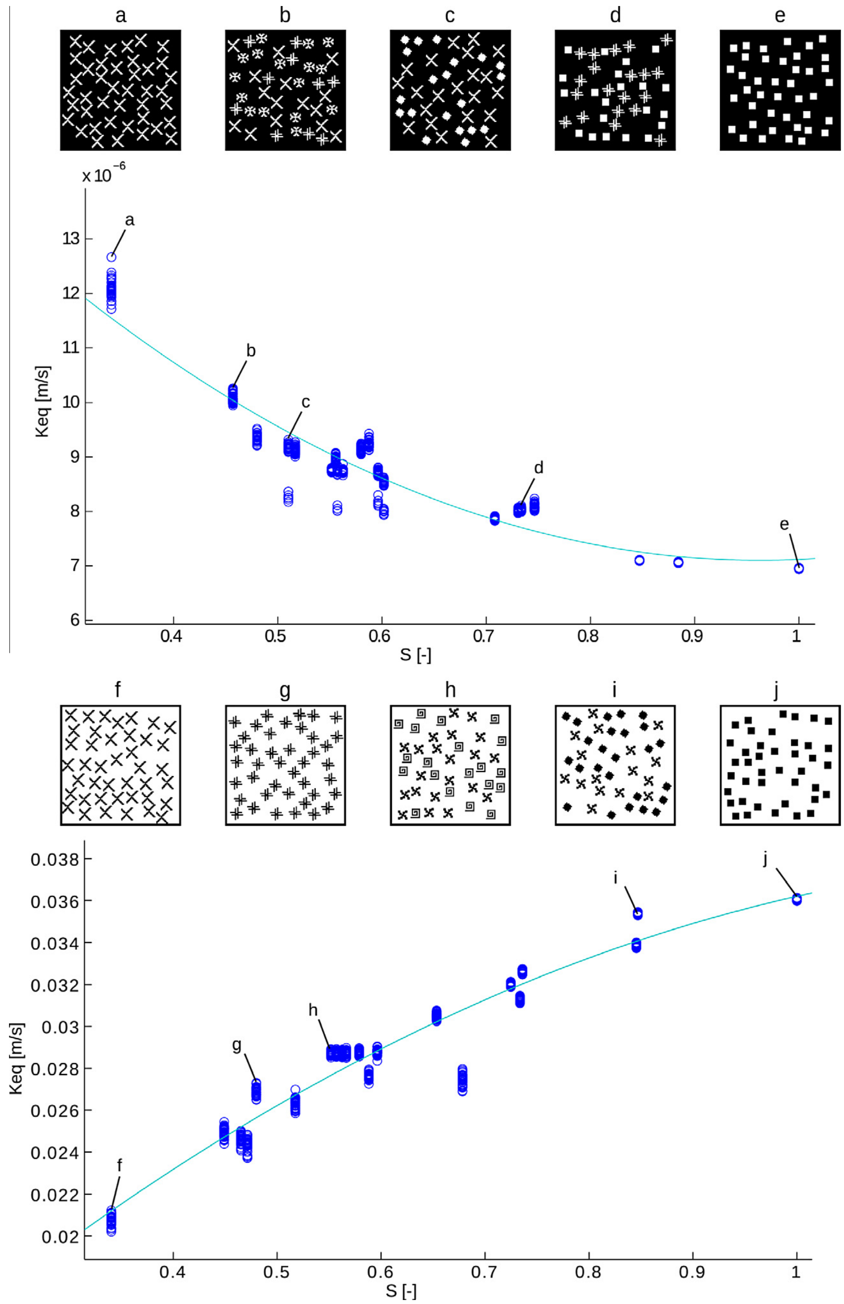

Fig. 3. Test 2, correlation between S and K_{eq} (geometric mean of x and y components). S is computed on *HP* inclusions (top) and on *LP* inclusions (bottom) respectively.

4. A new formula for the estimation of the equivalent conductivity

On the basis of the results obtained by the correlation studies shown in this paper (Section 3), we propose a new technique of K_{eq} estimation based on image analysis (K_{IA}).

According to bond percolation theory [39], increasing the probability of having an "open site" on a random infinite graph, large clusters of open sites begin to form until a specific threshold is reached (the *percolation threshold*) and an infinite path exists through the entire graph. This principle is applicable to binary random fields, where infinite connected components of both materials can exist or coexist. In the case of finite fields representative of an ergodic process, we can consider a connected component infinite if it touches two opposite borders of the field, this is called *infinite cluster* in the rest of the paper.

The Herrmann and Bernabé (*HB*) model [28], which inspires the new technique K_{IA}, is based on the quantification of the infinite cluster of the more conductive material (*HP*), which brings the primary contribution to the overall flow through the medium. In particular it is constituted by the following steps:

1. first it makes an estimation of the proportion of the total medium occupied by the infinite *HP* cluster based on a parametric power law derived from percolation theory [40];
2. then it considers the remaining part of the medium as a *HP*-*LP* mixture and approximates its equivalent conductivity using the lower Hashin–Shtrikman (*LHS*) bound [3];

3. finally it approximates the overall equivalent conductivity using the upper Hashin–Shtrikman (*UHS*) bound [3] of the resulting mixture.

As it has been discussed by Herrmann and Bernabé [29], the limits of this method are that it considers both the infinite *HP* cluster and the *HP-LP* mixture as statistically isotropic and homogeneous and it does not take into account any interaction between *HP* and *LP* materials. Furthermore, the quantification of the connected *HP* fraction based on the parametric approach needs to be calibrated over a range of experimental data and still shows large errors around the percolation threshold. On the contrary, the K_{IA} model features a direct identification of the infinite *HP* cluster via image analysis and operates a correction of the proportion substituting each inclusion with its convex hull. Moreover it applies the *HS* bounds approximation to the infinite cluster and the isolated part separately, considering them both mixtures of *HP* and *LP* materials. In this way, any parametric law and spatial measure is avoided, taking as inputs the field image and the conductivity value of the two materials only. The algorithm is described in details below (see also Fig. 4).

Let us consider a binary medium as represented by the spatial categorical variable $Z(\mathbf{x}) : \mathbb{N}^2 \mapsto \{0,1\}$ with $x_k = 1,\dots,N_k$ and $k = 1,2$; describing the local conductivity (0 = low conductivity, 1 = high conductivity) in two dimensions. The *HP* and *LP* materials can be defined as subsets of the finite discrete coordinate space $\mathcal{X} \subset \mathbb{N}^2$:

$$\begin{aligned} HP &= \{\mathbf{x} \in \mathcal{X} \mid Z(\mathbf{x}) = 1\} \\ LP &= \{\mathbf{x} \in \mathcal{X} \mid Z(\mathbf{x}) = 0\} \end{aligned} \tag{6}$$

Moreover, the *labeling* of a generic subset G of $\mathcal{X}$ (G may represent here the spatial distribution of a given material or a mixture of materials) is a transformation which assumes values in $\mathbf{i} = 1,2,\dots,I$ for each ith connected component CC_i of G and can be defined as follows:

$$L_G(\mathbf{x}) : \mathbb{N}^2 \mapsto \{0 \cup \mathbf{i}\} \qquad L_G(\mathbf{x}) = \begin{cases} i & \text{if} \quad \mathbf{x} \in CC_i \\ 0 & \text{if} \quad \mathbf{x} \notin G \end{cases} \tag{7}$$

Finally, the *convex hull transformation* of G, which is the set of convex hulls of each CC_i of G is defined as follows:

$$Conv(G) = \bigcup_{i=1}^{I} H_i \tag{8}$$

where H_i is the convex hull of CC_i.

Based on these definitions, given the same binary distribution $Z(\mathbf{x})$, the algorithm to estimate the kth principal component of the K_{eq} tensor consists of the following steps:

1. *HP* is labeled in order to distinguish its connected components: $L_{HP}(\mathbf{x})$;
2. the infinite *HP* cluster C is isolated looking at the labels (A and B) which are present on both the boundaries of the field perpendicular to the kth direction:

$$\begin{aligned} A &= \{L_{HP}(\mathbf{x}) \mid x_k = 1\} \\ B &= \{L_{HP}(\mathbf{x}) \mid x_k = N_k\} \\ C &= \{\mathbf{x} \in HP \mid L_{HP}(\mathbf{x}) \in (A \cap B) \wedge L_{HP}(\mathbf{x}) \neq 0\} \end{aligned} \tag{9}$$

3. the convex hull transformation is applied to C in order to approximate the area where the flow is influenced by its presence (this is a mixture of *LP* and *HP* materials): $C^* = Conv(C)$;
4. the proportion of *LP* in C^* is corrected extending *LP* to its convex hull transformation:

$$Z(Conv(LP \cap C^*)) = 0 \tag{10}$$

5. the equivalent conductivity K_c of C^* is approximated to the *UHS* bound [3]:

$$K_c = k_h + \frac{(1-p^*)}{\frac{1}{k_l - k_h} + \frac{p^*}{2k_h}} \tag{11}$$

where p^* is the proportion of *HP* in C^*;

6. the complement of C^* is considered the non-percolating part of the medium: $M = \bar{C}^*$;
7. the proportion of *HP* in M is corrected extending *HP* to its convex hull transformation:

$$Z(Conv(M \cap HP)) = 1 \tag{12}$$

8. the equivalent conductivity K_m of M is computed using the *LHS* bound [3]:

$$K_m = k_l + \frac{p}{\frac{1}{k_h - k_l} + \frac{(1-p)}{2k_l}} \tag{13}$$

where p is the proportion of *HP* in M;

9. finally, the estimated equivalent conductivity K_{IA} of the whole medium is approximated using again the *UHS* bound:

$$K_{IA} = K_c + \frac{(1-p_c)}{\frac{1}{K_m - K_c} + \frac{p_c}{2K_c}} \tag{14}$$

where p_c is the proportion of C^* with respect to the whole medium.

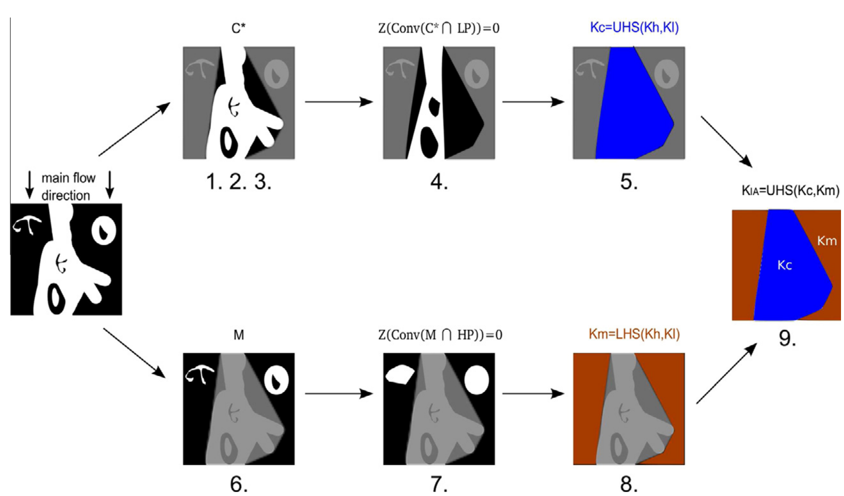

Fig. 4. Schematic illustration of the K_{IA} algorithm, the images show the result of each step, indicated by the corresponding number. The gray shading indicates parts that are not considered.

The algorithm is implemented in the matlab *KIA* package, freely available on request. The labeling and the convex hull substitution are performed using the matlab functions *bwlabel* and *bwconvhull* (Copyright 1984–2011 The MathWorks, Inc., based on [38,41]), according to the [8,4] connectivity criterion (see Section 2.3). This algorithm is applied to each direction, giving an estimation of the principal components of the K_{eq} tensor. In case of absence of the infinite *HP* cluster or the non-percolating zone ($C = \emptyset$ or $M = \emptyset$), a part of the process is avoided, directly imposing $K_{IA} = K_m$ or $K_{IA} = K_c$ respectively.

4.1. Estimation of K_{eq} on complex heterogeneities

The results of test 3 (Fig. 5) demonstrate the efficiency of the proposed method on a group of 400 Bernoulli fields covering the whole range of proportions *p*. HB^* refers to a modification of the *HB* model, necessary to apply to this type of field, not knowing all the parameters requested as input of the original algorithm. More precisely, it consists of making a direct quantification of the infinite *HP* cluster instead of using a parametric law, i.e. point 1 in *HB* algorithm is substituted by point 2 of the K_{IA} algorithm (see Section 4). The results of the HB^* model are clearly divided in two distinct groups (Fig. 5): K_{eq} is generally overestimated for the fields that present an infinite *HP* cluster (fields c,d,e,f for instance), while there is an underestimation for the ones which have not passed the percolation threshold (fields a and b). Results are clearly improved by the K_{IA} model, which incorporates the shape correction.

Test 4 (Fig. 7) is an attempt to verify the validity of the K_{IA} model on more complex geometries. Fig. 6 shows that the considered fields can have very different K_{eq} values for the same proportion and a wide range of the possible solutions is covered. There are two distinct groups of fields, corresponding mainly to $K_{eq}(x)$ values above 10^{-3} and below 10^{-4} respectively. The images of Fig. 7, linked to the alphabetical references in Fig. 6, suggest that this separation may be linked to the percolation threshold: fields $c,\ d,\ e$ and i present continuous *HP* (white) paths connecting the opposite borders in the horizontal direction, while fields a, b, f, g, h, j do not. Moreover, some evidence in support of the concepts presented in Section 3 is present: field *d* presents a *p* value slightly inferior to field *h* and *HP* have the same local level of connectedness in both fields (visually similar Euler number values). Nevertheless, *HP* is globally more connected in field *d*, being beyond the percolation threshold. This leads to a $keq(x)$ value one order of magnitude higher than in field *h*.

On the contrary, field *j* gives a similar result to *h* in terms of mean global flow although presenting a dramatically lower *p* value: this difference is compensated by the higher convexity of *HP* connected components (lower Solidity indicator) in *j*, having a positive influence on flow.

Fig. 7 shows that the K_{IA} model generally gives reasonable K_{eq} estimations, remaining in the same order of magnitude as the reference values obtained from the simulations. The less accurate estimations seem to correspond to fields in the proximity of the percolation threshold.

In terms of performance, for test 3, where the texture is finer and the morphological operations are more time demanding, the average computation time ratio between the numerical simulations and the K_{IA} model is 7.8. This means that the algorithm is at least 7 times faster than a numerical finite-elements flow simulation, without considering the pre- and post-processing operations needed by the latter. In regards to test 4, the complexity and the large quantity of the fields have demanded the use of a parallel-computing 64 cores cluster, taking several hours to solve the flow simulations. On the contrary, a linear matlab implementation of the K_{IA} model provides the estimation for all the fields in less than 1 h and a half, using an ordinary personal computer.

4.2. The role of inclusions shape in 3D

The flow through a three-dimensional medium is less constrained in 3D than in 2D, therefore the influence of the connected components shape on the global flow significantly depends on their orientation and its quantification is not straightforward. Let us consider, for example, a cross-shaped *LP* torus inclusion surrounded by a *HP* matrix, the global flow following the *x* direction as in Fig. 8. The hydrogeological parameterization and boundary conditions are the same as the previous experiments (see Sections 2.1 and 2.2). The chosen shape presents concavities in both the inner and the outer part, which are supposed to have a certain influence on the local flow of the convex region. There are two extreme cases for which the flow response is different according to the orientation of the inclusion:

1. In Fig. 8, case 1, the torus minor axis (*z* direction) is perpendicular to the main flow direction *x*. The local flow deviates as it encounters the outer surface of the inclusion. Consequently, lower velocity (blue–white) regions appear in the *x*-component of the specific flux field beside both inner and outer concavities of the torus.
2. In Fig. 8, case 2, the torus minor axis (*x* direction) is parallel to the main flow direction *x*. The fluid is free to pass through all the concavities without being perturbed by the surrounding *LP* material. The influence on the local flow in the nearby *HP* matrix is therefore minimal.

In the general case, a rule to recognize which part of the concavity influences the local flow can be the following: only concave surface portions non-parallel to the main flow direction generate a lower velocity region in the adjacent *HP* regions. For example, in case 1 (Fig. 8), a consistent portion of the concave surface is perpendicular to the main flow direction, having a clear influence on the local flow. As one can imagine, an even stronger influence is played by closed concave surfaces, e.g. the inside of a hollow sphere. Based on these observations, to estimate the *k*th K_{eq} component, a correction of the *LP* proportion accounting only for the convex hull of the concave surfaces non-parallel to the *k*th direction is needed. A good approximation of this concept is given by a novel image analysis operation called *pseudo-convex hull transformation*: it computes the union of the convex hull transformation of all the 2D sections normal to each principal direction, except the *k*th one. Let us consider a generic subset *G* of the 3D coordinate space $\mathbf{x} \in \mathbb{N}^3$ with $x_i = 1, \ldots, N_i$, being N_i the size of the domain in the *i*th direction. Following the notation of Section 4, the proposed operation is defined as follows:

$$Pconv(G,k) = \bigcup_{i \neq k} \bigcup_{j=1}^{N_i} Conv(G \cap \{x_i = j\}), \tag{15}$$

where $G \cap \{x_i = j\}$ is the *j*th 2D slice of *G*, normal to the direction *i*. The *k*th direction is excluded from the operation, being the one for which the parallel concavity has to be ignored.

Fig. 8 shows that the $Pconv(\cdot)$ transformation approximates fairly well the volume of influence on the local flow of the cross-shaped torus according to its orientation. In particular, in field 2, where all the concave surface is parallel to the *x* direction, no volume augmentation occurs, reflecting the almost null influence of the concavity on the local flow. Fig. 9 illustrates the efficiency of the operator on a more complex shape: again, only the concave portions of surface non-parallel to the main flow direction produce a low velocity area, which is approximated by the $Pconv(\cdot)$ transformation. Finally, it has to be remarked that for closed concave surfaces $Conv(\cdot)$ and $Pconv(\cdot)$ have the same result.

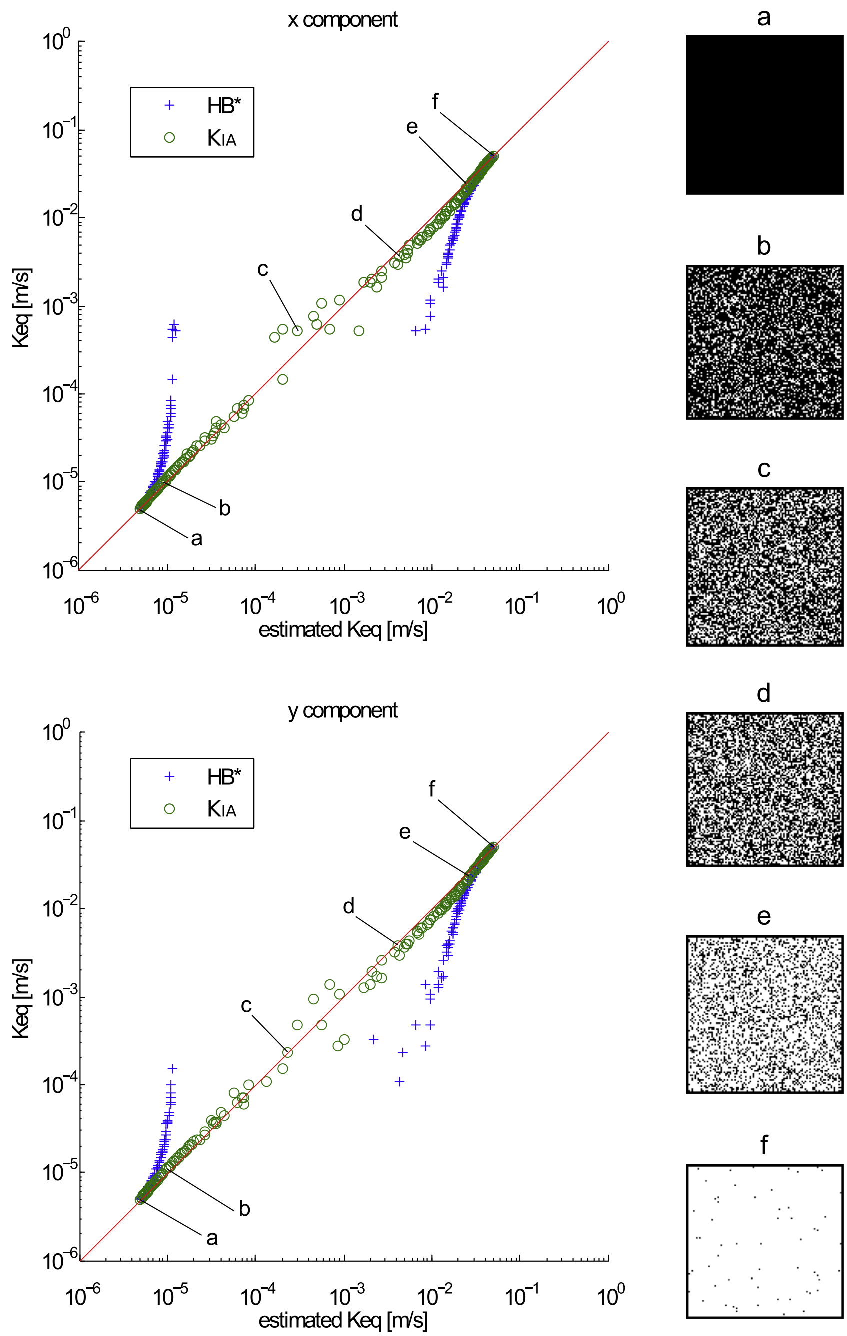

Fig. 5. Test 3, scatter-plot of the reference K_{eq} values as a function of the estimated ones, using the K_{IA} model and the HB^* model. The bisector line indicates the exact estimation. Some examples of the fields are shown on the right, with link to the corresponding data.

The principle described above is restricted to *LP* inclusions, since the influence of *HP* inclusions shape on the nearby *LP* matrix is radically different. Fig. 10 shows the same type of fields of Fig. 8 but with an inversion of the materials. The influence of the concavity itself on the local flow does not vary significantly with the orientation, in both cases the concavity does not generate a high velocity region in the nearby *HP* matrix. On the contrary, the orientation of the whole inclusion has an influence on the local flow: when it is elongated towards the main flow direction (field 1), the local flow is canalized into the inclusion and a higher velocity path forms. This effect is negligible on statistically isotropic fields, since the local anisotropy is averaged over the global hydrofacies distribution, i.e. there is not a predominant orientation of the connected components. Anyway, as shown in 2D (see Section 2.4), the level of concavity of *HP* inclusions is still supposed to play a significant role in 3D, reducing the distance between each others, thus incrementing the presence of higher velocity paths. For this reason, the $Conv(\cdot)$ transformation can still be applied to the *LP* inclusions in 3D.

4.3. The role of the infinite cluster in 3D

The presence of the infinite cluster still plays a significant role in 3D fields, as it implies a sharp augmentation of the K_{eq} value. Similarly to the 2D case, the infinite cluster can be detected and isolated from the rest of the field using a 3D labeling function, but only a limited part of it corresponds to higher velocity flow paths. Let us consider for example the conductivity field of

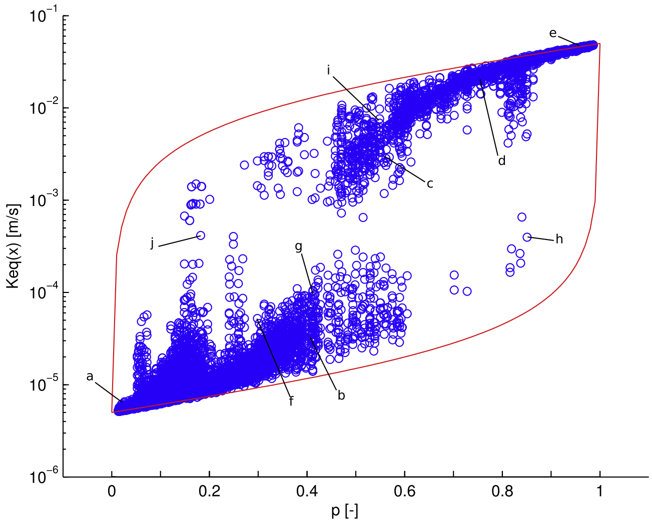

Fig. 6. Test 4, scatter-plot of the x component of K_{eq} as a function of p (proportion of the more conductive hydrofacies). The two curves represent the *HS* bounds. The alphabetical references correspond to the fields in Fig. 7.

Fig. 11, on which the flow field has been computed with the main flow direction following x, the hydrogeological parameterization and boundary conditions being the same of the previous experiments (see Sections 2.1 and 2.2). The *HP* material inside the infinite cluster occupies 75% of the total field, while only 16% is constituted by higher velocity regions ($v_x \geqslant 0.05$ (m/s)). Moreover, the figure shows that these regions correspond to portions of the infinite cluster where the section perpendicular to the local flow direction is reduced. In other words, the higher velocity flow paths are limited by the presence of bottlenecks inside the *HP* material of the infinite cluster, therefore the *HP* proportion needs to be conveniently reduced in order to quantify the actual fraction of the medium which allows a high velocity percolation process. In 2D, this is achieved by applying the convex hull transformation of the *LP* material inside the infinite cluster (point 4 of the K_{IA} algorithm). This operation leads to accurate K_{eq} estimations on isotropic fields, but it is not applicable on the 3D case, since it may lead to consider a *LP* region fully surrounding the *HP* material and causing the total cancelation of the latter. Finding an efficient way to correct the *HP* proportion (p^*) inside the infinite cluster is not trivial, a first approximation proposed in this paper is to consider the minimum p value found among all 2D sections perpendicular to the considered flow direction. Let us consider a generic subset G, representing the infinite cluster, of the 3D coordinate space $\mathbf{x} \in \mathbb{N}^3$ with

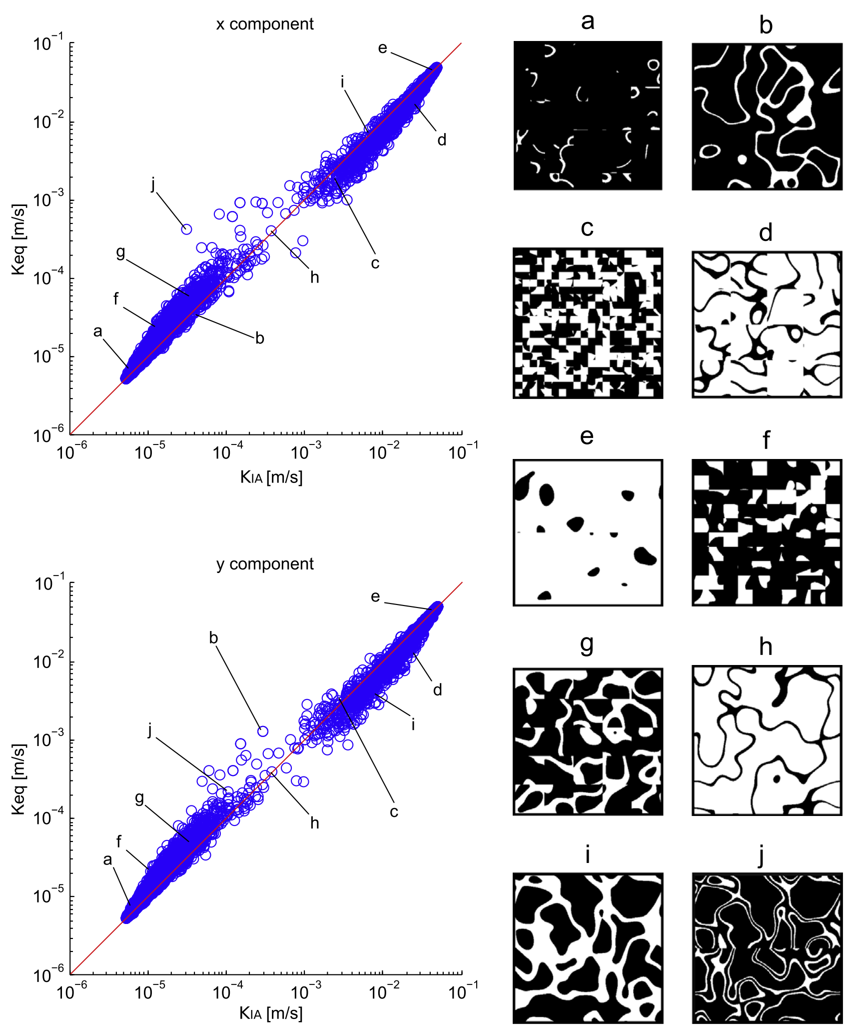

Fig. 7. Test 4, scatter-plot of the reference K_{eq} values as a function of the estimated ones, using the K_{IA} model. The bisector line indicates the exact estimation. Some examples of the fields are shown on the right, with link to the corresponding data.

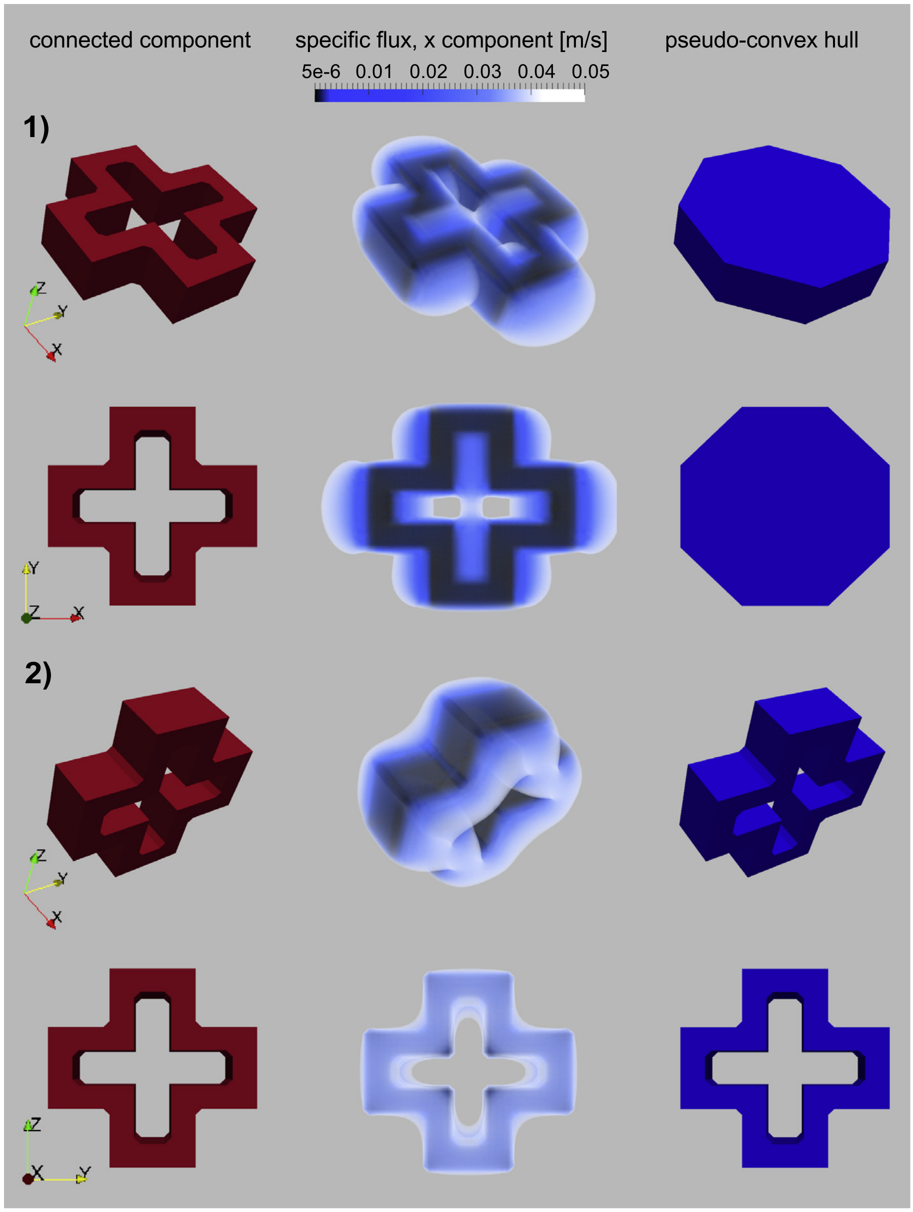

Fig. 8. 3D image of a cross-shaped-torus *LP* inclusion surrounded by a *HP* matrix (non-visible), its minor axis being parallel to: (1) the *z* direction and (2) the *x* direction. In both cases, the pseudo-convex hull transformation $Pconv(LP, x)$ and the specific flux *x*-component v_x are shown. The main flow direction is *x*. For a matter of visibility, regions presenting $v_x > 0.04$ (m/s) (undisturbed *HP* matrix) are omitted from the flow field image.

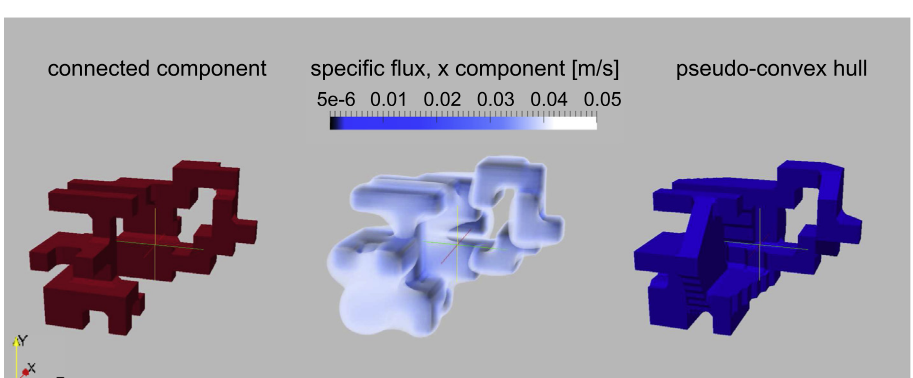

Fig. 9. 3D image of a *LP* inclusion surrounded by a *HP* matrix (non-visible). The pseudo-convex hull transformation $Pconv(LP, x)$ and the specific flux *x*-component v_x are shown. The main flow direction is *x*. For a matter of visibility, regions presenting $v_x > 0.04$ (m/s) (undisturbed *HP* matrix) are omitted from the flow field image.

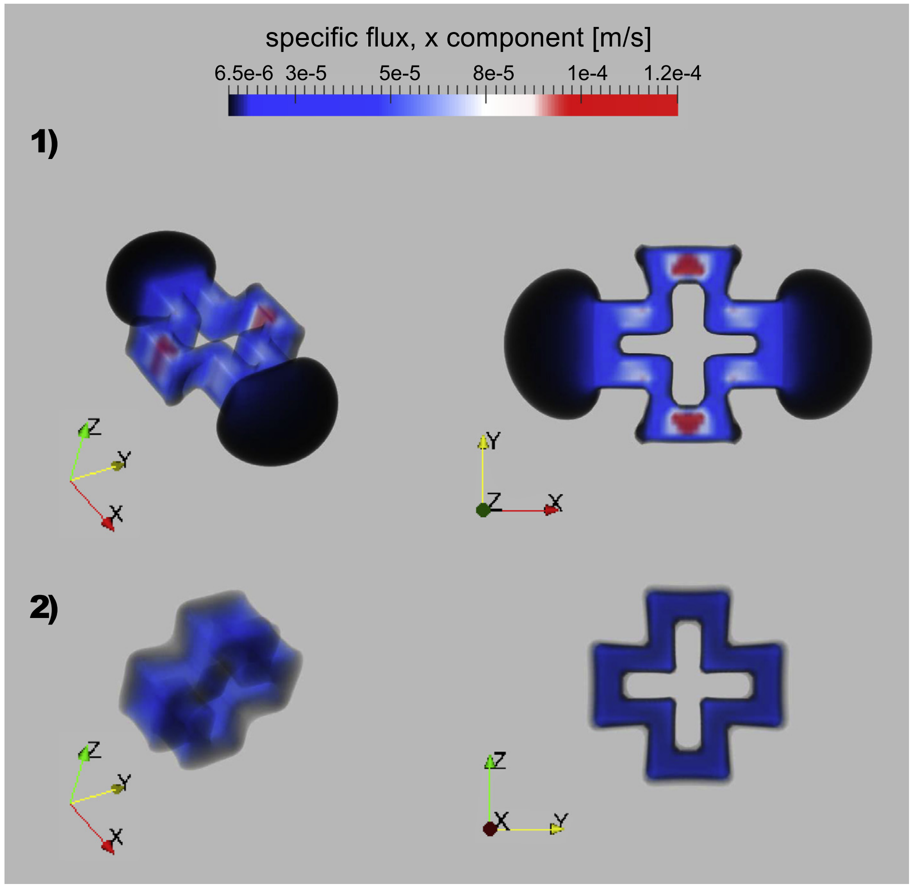

Fig. 10. 3D image of a cross-shaped-torus *HP* inclusion surrounded by a *LP* matrix (non-visible), its minor axis being parallel to: (1) the *z* direction and (2) the *x* direction. In both cases, the specific flux *x*-component v_x is shown. The main flow direction is *x*. For a matter of visibility, regions presenting $v_x < 6.5 \times 10^{-06}$ (m/s) (undisturbed *LP* matrix) are omitted from the flow field image.

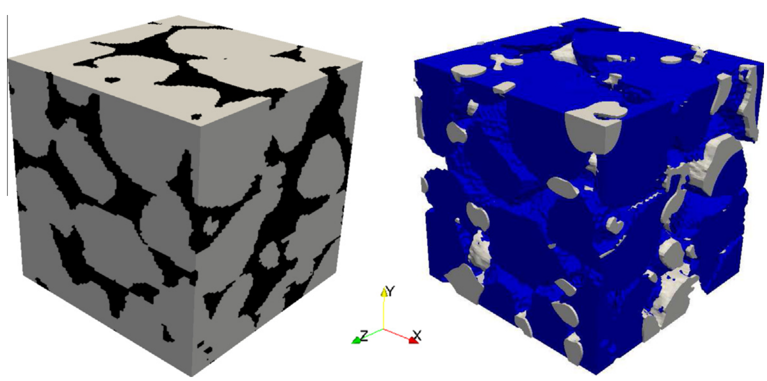

Fig. 11. Example of a 3D binary field presenting a large infinite cluster: *LP* (black) and *HP* (white) materials distributions on the left, *HP* material (blue) and higher velocity regions (gray) on the right, obtained from a flow simulation along the *x* direction and isolating the regions with $v_x \geqslant 0.05$ (m/s). (For interpretation of the references to color in this figure legend, the reader is referred to the web version of this article.)

$x_k = 1, \ldots, N_k$ and $k = 1, 2, 3$. The correction of G to estimate the kth K_{eq} component is defined as follows:

$$p^* = min\{p(G \cap \{x_k = j\})\}; \quad j = 1, \ldots, N_k; \tag{16}$$

where $p(\cdot)$ is the computation of the *HP* proportion and N_k the dimension of the domain along k. In this way, the proportion of the infinite cluster is reduced considering the presence of bottlenecks.

4.4. An early 3D implementation

To test the validity of the principles established in Sections 4.2 and 4.3, and following the notation of Section 4, an early 3D version of the K_{IA} algorithm is proposed here.

Let us consider a 3D binary medium as represented by the spatial categorical variable $Z(\mathbf{x}) : \mathbb{N}^3 \mapsto \{0, 1\}$ with $x_k = 1, \ldots, N_k$ and $k = 1, 2, 3$; describing the local conductivity (0 = low conductivity, 1 = high conductivity). The estimation of the kth principal component of the K_{eq} tensor consists of the following steps:

1. HP is labeled in order to distinguish its connected components: $L_{HP}(\mathbf{x})$;
2. the infinite HP cluster C is isolated looking at the labels (A and B) which are present on both the boundaries of the field perpendicular to the kth direction:

$$\begin{aligned} A &= \{L_{HP}(\mathbf{x}) \mid x_k = 1\} \\ B &= \{L_{HP}(\mathbf{x}) \mid x_k = N_k\} \\ C &= \{\mathbf{x} \in HP \mid L_{HP}(\mathbf{x}) \in (A \cap B) \wedge L_{HP}(\mathbf{x}) \neq 0\} \end{aligned} \tag{17}$$

3. LP is labeled as well: $L_{LP}(\mathbf{x})$
4. the LP inclusions F are isolated looking at the labels which are absent from both the field boundaries (D and E) perpendicular to the kth direction:

$$\begin{aligned} D &= \{L_{LP}(\mathbf{x}) \mid x_k = 1\} \\ E &= \{L_{LP}(\mathbf{x}) \mid x_k = N_k\} \\ F &= \{\mathbf{x} \in LP \mid L_{LP}(\mathbf{x}) \notin (D \cup E) \wedge L_{LP}(\mathbf{x}) \neq 0\} \end{aligned} \tag{18}$$

5. the proportion of F is corrected extending it to its pseudo-convex hull transformation:

$$Z(Pconv(F,k)) = 0 \tag{19}$$

6. the convex hull transformation is applied to C in order to approximate the area where the flow is influenced by its presence (this is a mixture of LP and HP materials):

$$C^* = Conv(C)$$

7. the HP proportion p^* in the infinite cluster C^* is calculated with the following formula:

$$p^* = min\{p(C^* \cap \{x_k = j\}); \quad j = 1, \ldots, N_k; \tag{20}$$

8. the equivalent conductivity K_c of C^* is approximated to the UHS bound [3]:

$$K_c = k_h + \frac{(1-p^*)}{\frac{1}{k_l - k_h} + \frac{p^*}{3k_h}} \tag{21}$$

9. the complement of C^* is considered the non-percolating part of the medium: $M = \bar{C}^*$
10. the proportion of HP in M is corrected extending HP to its convex hull transformation:

$$Z(Conv(M \cap HP)) = 1 \tag{22}$$

11. the equivalent conductivity K_m of M is computed using the LHS bound [3]:

$$K_m = k_l + \frac{p}{\frac{1}{k_h - k_l} + \frac{(1-p)}{3k_l}} \tag{23}$$

where p is the proportion of HP in M;

12. finally, the estimated equivalent conductivity K_{IA} of the whole medium is approximated using again UHS bound:

$$K_{IA} = K_c + \frac{(1-p_c)}{\frac{1}{K_m - K_c} + \frac{p_c}{3K_c}} \tag{24}$$

where p_c is the proportion of C^* with respect to the whole medium.

In case of $C = \emptyset$ or $M = \emptyset$, a part of the process is avoided, directly imposing $K_{IA} = K_m$ or $K_{IA} = K_c$ respectively. The constant in the HS bounds formula is changed according to the dimensionality.

The algorithm is part of the matlab *KIA* package, freely available on request. The 3D labeling is performed using the matlab function *bwlabeln* (Copyright 1984–2011 The MathWorks, Inc., based on [42]) and the 3D computation of the convex hull is based on [38], according to the [26,6] connectivity criterion (see Section 2.3).

Test 5 (Fig. 12) checks the validity of the K_{IA} algorithm on 3D natural isotropic heterogeneities (see Section 2.1). The given K_{eq} estimation are less accurate than in the 2D case, although generally remaining in the same order of magnitude of the reference. In particular, fields constituted by a LP matrix and HP inclusions or vice versa (K_{eq} values toward the extremes) show more accurate estimations, confirming the validity of the operations applied to this type of fields. On the contrary, fields closer to the percolation threshold (reference values around 10^{-3}) present a more consistent overestimation of K_{eq}. This result suggests that a more efficient image analysis operation is needed to correct the proportion of the infinite cluster. In particular, the overestimation may be due to the fact that p^* is quantified considering a whole 2D section of C^*, instead of being restricted to the portions corresponding effectively to direct paths connecting the two opposite boundaries of the field. For this purpose, a future aim is to find a combination of fast and robust image analysis operations to select the minimum diameter found on each percolating branch of C^* and derive from it a more correct p^* value.

5. Conclusions

The aim of this work was to analyze the influence of the geometry and the topology on the equivalent hydraulic conductivity (K_{eq}) of binary media, since in many cases the measure of the proportion of the hydrofacies is not sufficient to make a reliable K_{eq} estimation.

The correlation between the Euler number and K_{eq} has been tested on a large group of more than 900 isotropic fields presenting low permeability inclusions in a highly permeable matrix and vice versa, keeping constant the proportion and the shape of the hydrofacies. The results have shown a bad correlation between the Euler number and K_{eq}, with a small variability of K_{eq} being primarily controlled by the relative position of the inclusions, as already described by Knudby et al. [26]. This is a clear signal that a pure topological connectivity measure may not be suitable to catch the connectedness related to flow properties. Moreover, this result demonstrates that any local measure solely based on the number of connected components or on the neighborhood of each pixel cannot catch the global level of connectedness of the medium, which is the main factor of control of the global flux after the proportion of the hydrofacies.

The Solidity indicator, calculated for each connected component as the ratio between its area and the area of its convex hull, has presented an interesting non-linear correlation with K_{eq} that was not discussed previously to our knowledge. This relationship shows that the area of influence of each inclusion is related to its convex hull, as one can intuitively expect.

In order to verify the validity of these principles, a new model of estimation of the equivalent conductivity based on Image Analysis (K_{IA}) has been proposed. Its most important features are: (i) the direct quantification of the connected fraction against the unconnected one; (ii) the substitution of each inclusion by its convex hull. In this way, the estimation takes into account three fundamental aspects of the spatial distribution: the proportion of the hydrofacies, the connectivity and the geometry of the inclusions. The resulting model, tested on 400 Bernoulli fields and 10,216 fields presenting a great variety of geometries, shows a good reliability and numerical efficiency on isotropic 2D fields.

The proposed 3D version of the K_{IA} algorithm is based on the same main principles as the 2D implementation, with the introduction of two different image analysis operations: (i) the pseudo-convex hull transformation to account for the different behavior of the low permeability inclusions and (ii) a correction of the highly permeable material proportion inside the percolating cluster, based on the minimum value found on the 2D sections normal to the considered flow direction. The latter operation is just a first approximation of a more complex analysis that should take

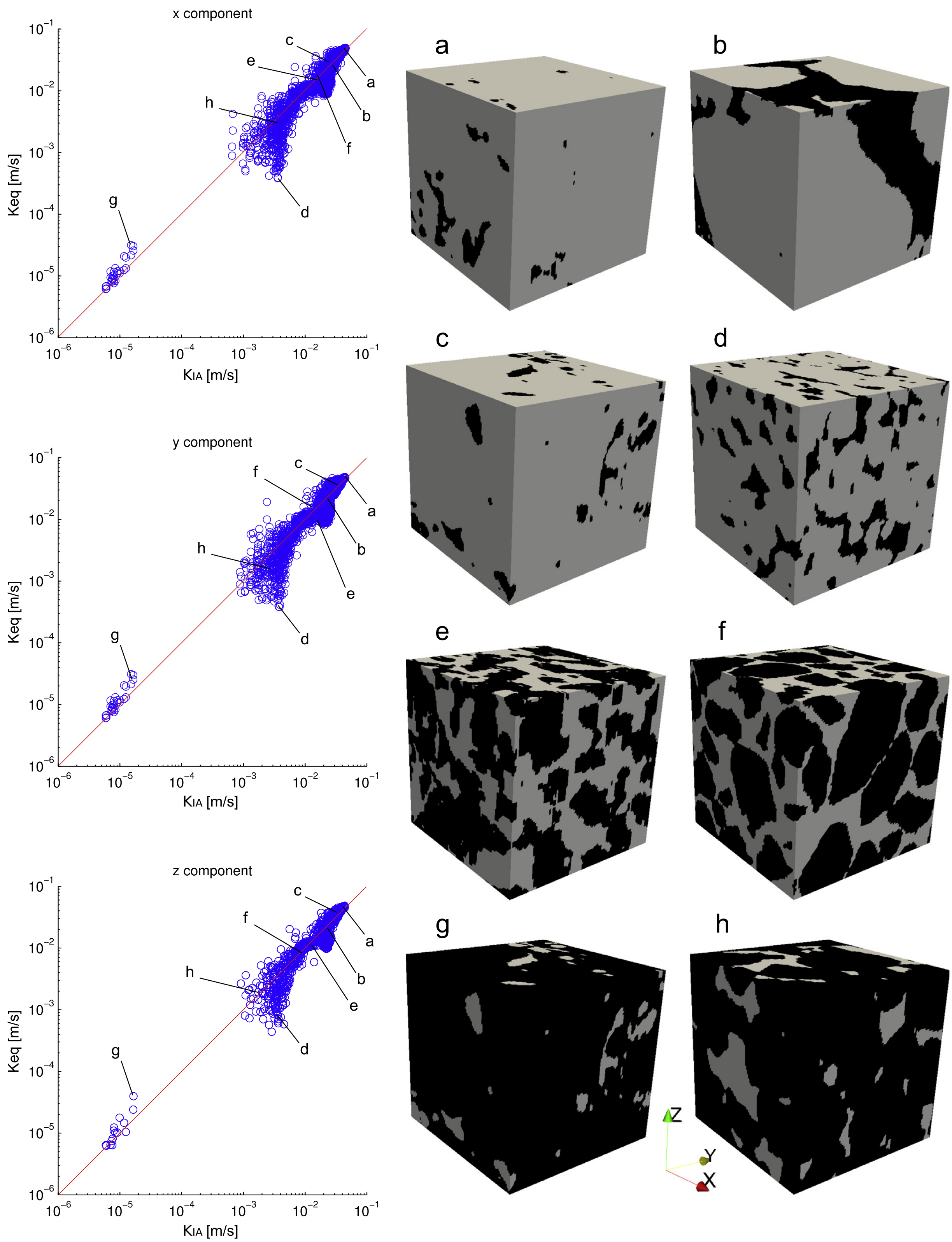

Fig. 12. Test 5, scatter-plot of the reference K_{eq} values as a function of the estimated ones, using the K_{IA} model. The bisector line indicates the exact estimation. Some examples of the fields are shown on the right.

into account each branch of the percolating cluster separately. The algorithm, tested on 2196 fields presenting natural isotropic heterogeneities, shows lower accuracy in the estimations as compared to the 2D version, but it demonstrates that the proposed principles are still valid in 3D. A future development of the algorithm could include a more efficient image analysis operation for the correction of the highly permeable material inside the percolating cluster and the extension of its applicability to anisotropic fields.

References

[1] Samouelian A, Vogel HJ, Ippisch O. Upscaling hydraulic conductivity based on the topology of the sub-scale structure. Adv Water Resour 2007;30(5):1179–89. http://dx.doi.org/10.1016/j.advwatres.2006.10.011.

[2] Wiener O. Die theorie des mischkorpers für das feld der stationaren stromung abh sach. Ges Wiss Math Phys K 1912;32:509.

[3] Hashin Z, Shtrikman S. A variational approach to theory of effective magnetic permeability of multiphase materials. J Appl Phys 1962;33(10):3125–31. http://dx.doi.org/10.1063/1.1728579.

[4] Maxwell JC. A treatise on electricity and magnetism, vol. 1. Clarendon Press; 1873.

[5] Matheron G. Eléments pour une théorie des milieux poreux, vol. 164. Paris: Masson; 1967.

[6] Dagan G. Models of groundwater flow in statistically homogeneous porous formations. Water Resour Res 1979;15(1):47–63. http://dx.doi.org/10.1029/WR015i001p00047.

[7] Dagan G. Theory of flow and transport in porous formations. Springer-Verlag; 1989, ISBN 9780387510989. http://dx.doi.org/10.1007/978-3-642-75015-1.

[8] Rubin Y. Flow and transport in bimodal heterogeneous formations. Water Resour Res 1995;31(10):2461–8. http://dx.doi.org/10.1029/95WR01953.

[9] Jankovic I, Fiori A, Dagan G. Effective conductivity of an isotropic heterogeneous medium of lognormal conductivity distribution. Multiscale Model Simul 2003;1(1). http://dx.doi.org/10.1137/S1540345902409633 (PII: S1540345902409633).

[10] Fiori A, Jankovic I, Dagan G. Effective conductivity of heterogeneous multiphase media with circular inclusions. Phys Rev Lett 2005;94(22):224502. http://dx.doi.org/10.1103/PhysRevLett. 94.224502.

[11] Firmani G, Fiori A, Jankovic I, Dagan G. Effective conductivity of random multiphase 2d media with polydisperse circular inclusions. Multiscale Model Simul 2009;7(4):1979–2001. http://dx.doi.org/10.1137/080734376.

[12] Duan HL, Karihaloo BL, Wang J, Yi X. Effective conductivities of heterogeneous media containing multiple inclusions with various spatial distributions. Phys Rev B 2006;73(17):174203. http://dx.doi.org/10.1103/PhysRevB.73.174203.

[13] Yeh TCJ, Gelhar LW, Gutjahr AL. Stochastic-analysis of unsaturated flow in heterogeneous soils. 2: Statistically anisotropic media with variable-alpha. Water Resour Res 1985;21(4):457–64. http://dx.doi.org/10.1029/WR021i004p00457.

[14] Khaleel R, Yeh TCJ, Lu ZM. Upscaled flow and transport properties for heterogeneous unsaturated media. Water Resour Res 2002;38(5):1053. http://dx.doi.org/10.1029/2000WR000072.

[15] Journel A, Deutsch C, Desbarats A. Power averaging for block effective permeability. In: SPE California Regional Meeting; 1986. http://dx.doi.org/10.2118/15128-MS.

[16] Hornung U. Homogenization and porous media. Springer Verlag; 1997, ISBN 0387947868. http://dx.doi.org/10.1007/978-1-4612-1920-0.

[17] King PR. The use of renormalization for calculating effective permeability. Transp Porous Med 1989;4(1):37–58. http://dx.doi.org/10.1007/BF00134741.

[18] Renard P, Le Loc'h G, Ledoux E, de Marsily G, Mackay R. A fast algorithm for the estimation of the equivalent hydraulic conductivity of heterogeneous media. Water Resour Res 2000;36(12):3567–80. http://dx.doi.org/10.1029/2000WR900203.

[19] Sanchez-Vila X, Guadagnini A, Carrera J. Representative hydraulic conductivities in saturated groundwater flow. Rev Geophys 2006;44(3):RG3002. http://dx.doi.org/10.1029/2005RG000169.

[20] Renard P, de Marsily G. Calculating equivalent permeability: a review. Adv Water Resour 1997;20(5–6):253–78. http://dx.doi.org/10.1016/S0309-1708(96)00050-4.

[21] Vogel HJ. Topological characterization of porous media. In: Mecke K, Stoyan D, editors. Morphology of condensed matter. Lecture notes in physics, vol. 600. Berlin, Heidelberg: Springer; 2002, ISBN 978-3-540-44203-5. p. 75–92. http://dx.doi.org/10.1007/3-540-45782-83.

[22] Zinn B, Harvey CF. When good statistical models of aquifer heterogeneity go bad: a comparison of flow, dispersion, and mass transfer in connected and multivariate gaussian hydraulic conductivity fields. Water Resour Res 2003;39(3):1051. http://dx.doi.org/10.1029/2001WR001146.

[23] Neuweiler I, Cirpka OA. Homogenization of richards equation in permeability fields with different connectivities. Water Resour Res 2005;41(2):W02009. http://dx.doi.org/10.1029/2004WR003329.

[24] Knudby C, Carrera J. On the relationship between indicators of geostatistical, flow and transport connectivity. Adv Water Resour 2005;28(4):405–21. http://dx.doi.org/10.1016/j.advwatres.2004.09.001.

[25] Renard P, Allard D. Connectivity metrics for subsurface flow and transport. Adv Water Resour 2013;51:168–96. http://dx.doi.org/10.1016/j.advwatres.2011.12.001.

[26] Knudby C, Carrera J, Bumgardner JD, Fogg GE. Binary upscaling – the role of connectivity and a new formula. Adv Water Resour 2006;29(4):590–604. http://dx.doi.org/10.1016/j.advwatres.2005.07.002.

[27] Bumgardner J. Characterization of effective hydraulic conductivity in sand-clay mixtures [Ph.D. thesis]. U. of Calif.; 1990.

[28] Herrmann FJ, Bernabe Y. Seismic singularities at upper-mantle phase transitions: a site percolation model. Geophys J Int 2004;159(3):949–60. http://dx.doi.org/10.1111/j.1365-246X.2004.02464.x.

[29] Bernabe Y, Mok U, Evans B, Herrmann FJ. Permeability and storativity of binary mixtures of high- and low-permeability materials. J Geophys Res – Solid Earth 2004;109(B12):B12207. http://dx.doi.org/10.1029/2004JB003111.

[30] Dong H. Micro ct imaging and pore network extraction [Ph.D. thesis]. Department of Earth Science and Engineering, Imperial College of London; 2007.

[31] Rubin Y, Gomezhernandez JJ. A stochastic approach to the problem of upscaling of conductivity in disordered media – theory and unconditional numerical simulations. Water Resour Res 1990;26(4):691–701. http://dx.doi.org/10.1029/WR026i004p00691.

[32] Cornaton F. Ground water (GW)(version 1.4.1) a 3-d ground water flow, mass transport and heat transfer finite element simulator. University of Neuchatel, Switzerland; 2010.

[33] Rosenfeld A. Digital topology. Am Math Mon 1979;86(8):621–30. http://dx.doi.org/10.2307/2321290.

[34] Veblen O. Theory on plane curves in non-metrical analysis situs. Trans Am Math Soc 1905;6(1):83–98. http://dx.doi.org/10.2307/1986378.

[35] Hadwiger H. Vorlesungen über inhalt, Oberfläche und isoperimetrie, vol. 93. Berlin: Springer; 1957. http://dx.doi.org/10.1007/978-3-642-94702-5.

[36] Pratt W. Digital image processing. Wiley; 1991.

[37] Gray S. Local properties of binary images in two dimensions. IEEE Trans Comput 1971;100(5):551–61. http://dx.doi.org/10.1109/T-C.1971.223289.

[38] Barber CB, Dobkin DP, Huhdanpaa H. The quickhull algorithm for convex hulls. ACM Trans Math Softw 1996;22(4):469–83. http://dx.doi.org/10.1145/235815.235821.

[39] Broadbent SR, Hammersley JM. Percolation processes. Math Proc Cambridge Philos Soc 1957;53:629–41. http://dx.doi.org/10.1017/S0305004100032680.

[40] Stauffer D, Aharony A. Introduction to percolation theory. London: Taylor and Francis; 1992, ISBN 978-0-7484-0027-0.

[41] Haralick RM, Shapiro LG. Computer and robot vision, vol. 1. Addison-Wesley; 1992, ISBN 978-0-201-10877-4.

[42] Sedgewick R. Algorithms in C. Addison-Wesley; 1998, ISBN 978-0-201-51425-4.